Ann. Occup. Hyg., Vol. 57, No. 9, pp. 1148–1166, 2013

doi:10.1093/annhyg/met042

Properties that Influence the Specific Surface Areas of Carbon Nanotubes and Nanofibers

M. EILEEN BIRCH[1]*, TONI A. RUDA-EBERENZ[2], MING CHAI[3], RONNEE ANDREWS[1] and RANDAL L. HATFIELD[4]

[1]US Department of Health and Human Services, Public Health Service, Centers for Disease Control and Prevention, National Institute for Occupational Safety and Health, Division of Applied Research and Technology, MS-R7 4676 Columbia Parkway, Cincinnati, OH 45226, USA; [4]Pacific Surface Science Inc., 1617 Pacific Avenue Unit 114, Oxnard, CA 93033, USA

Received 6 February 2013; in final form 14 June 2013; accepted 24 June 2013; Advance Access publication 12 September 2013

Commercially available carbon nanotubes and nanofibers were analyzed to examine possible relationships between their Brunauer–Emmett–Teller specific surface areas (SSAs) and their physical and chemical properties. Properties found to influence surface area were number of walls/diameter, impurities, and surface functionalization with hydroxyl and carboxyl groups. Characterization by electron microscopy, energy-dispersive X-ray spectrometry, thermogravimetric analysis, and elemental analysis indicates that SSA can provide insight on carbon nanomaterials properties, which can differ vastly depending on synthesis parameters and post-production treatments. In this study, how different properties may influence surface area is discussed. The materials examined have a wide range of surface areas. The measured surface areas differed from product specifications, to varying degrees, and between similar products. Findings emphasize the multiple factors that influence surface area and mark its utility in carbon nanomaterial characterization, a prerequisite to understanding their potential applications and toxicities. Implications for occupational monitoring are discussed.

Keywords: BET-specific surface area; carbon nanotube; nanofiber; nanomaterial

INTRODUCTION

The potential applications of graphene-based materials such as carbon nanotubes (CNTs) and carbon nanofibers (CNFs) are being extensively studied. Currently, CNTs and CNFs are produced/used in a range of facilities, from small-scale research laboratories to industrial-scale production plants. Current applications include electronics, batteries, solar cells, polymer composites, coatings, inks, adhesives, and biomedical devices (WTEC, 2007; Milne *et al*., 2008); substantial market growth for CNTs/CNFs is expected over the next decade (Lux Research, 2007).

Increasing production of CNTs and CNFs may pose risks for workers who process these materials. Adverse respiratory and systemic effects have been found in animal studies (Lam *et al*., 2004; Muller *et al*., 2005; Shvedova *et al*., 2003, 2005, 2008; Lison and Muller, 2008; Poland *et al*., 2008; Mercer *et al*., 2009; Nurkiewicz *et al*. 2009; Pauluhn, 2010; Porter *et al*., 2010; Mercer *et al*., 2011; Murray *et al*., 2012), indicating the need to limit worker exposure. CNTs with a nickel content of 26% (Lam *et al*., 2004) and those with higher (18% versus 0.2%) iron content (Shvedova *et al*.,

*Author to whom correspondence should be addressed. Tel: +1-513-841-4298; fax: +1-513-841-4545; e-mail: mib2@cdc.gov
[2]Present address: 2309A Sandy Plains Road, Clarksville, PA 15322, USA.
[3]Present address: Bluegrass Biodiesel, 175 David Pribble Drive, Falmouth, KY 41040, USA.

2003, 2008) were reportedly more cytotoxic, but both purified and unpurified CNTs caused adverse lung effects (Lam *et al*., 2004; Shvedova *et al*., 2005, 2008). Early onset and persistent fibrosis (Shvedova *et al*., 2005, 2008; Porter *et al*., 2010; Mercer *et al*., 2011), pulmonary inflammation and fibrosis (Lam *et al*., 2004; Muller *et al*., 2005; Shvedova *et al*., 2005), and reduced lung clearance (Mercer *et al*., 2009; Pauluhn, 2010) have been observed in rodents at relatively low-mass doses. Acute pulmonary inflammation and interstitial fibrosis also have been observed in mice exposed to CNFs (Murray *et al*., 2012). More alarming is the prospect of asbestos-like pathology, as reported for one type of multi-walled CNTs (MWCNTs) injected into the abdominal cavities of mice (Poland *et al*., 2008).

CNTs and CNFs can have vastly different properties, depending on synthesis parameters and post-production treatments. The varying properties may have significant impact on CNT/CNF toxicity (Donaldson *et al*., 2006), making it difficult to assess the health risks of these materials. Though the mechanisms of toxicity are unclear, health-relevant properties may include fiber/tube length, diameter, durability, and chirality; metal impurities (from catalysts); agglomerate/bundle size, structure and morphology; and surface area. In particular, interest in surface area is based on toxicological studies on some types of insoluble nanoscale materials, wherein surface area was found to be better correlated with biological response than mass (Lison *et al*. 1997; Tran *et al*., 2000; Brown *et al*., 2001; Oberdörster *et al*., 2005; Nel *et al*., 2006; Stoeger *et al*., 2006; Monteiller *et al*., 2007; Singh *et al*., 2007; Nurkiewicz *et al*., 2009; Sager and Castranova, 2009; LeBlanc *et al*., 2010). Better correlation may relate to the greater surface reactivity (Hsieh *et al*., 2012) (e.g. inflammatory potential) of smaller particles per unit mass relative to larger (micrometer) ones.

CNTs have large surface areas because of their structure and physical form. A theoretical surface area of 1315 m^2g^{-1} has been estimated for discrete, single-walled CNTs (SWCNTs) assumed to be closed (i.e. no access to tube interior; Peigney *et al*., 2001). Their actual surface areas may be influenced by a variety of properties such as tube/fiber diameter, bundling and agglomeration, purity, and surface functionalization. For example, as a result of fiber bundling and impurities, the measured surface areas of SWCNTs are typically much lower than theoretical, often 600 m^2g^{-1} or less. Theoretical surface areas for MWCNTs are diameter-dependent and estimated to be a few 100 m^2g^{-1} (Peigney *et al*., 2001), reflective of their actual surface areas.

This paper examines the relationship between the surface areas of commercially available CNT and CNF products and their physical and chemical properties. Specific surface area (SSA) was determined by the Brunauer–Emmett–Teller (BET) gas adsorption method, the most widely used method for SSA. To support some of the conclusions drawn, structural and elemental composition data on the materials were obtained by scanning electron microscopy (SEM) with energy-dispersive X-ray spectrometry (EDS) and transmission electron microscopy (TEM) with EDS. Further elemental data were obtained by inductively coupled plasma atomic emission spectroscopy (ICP-AES). Thermogravimetric analysis (TGA) was also performed to provide supplemental information. This study focuses on CNTs, but several raw (unprocessed) and processed CNFs also were examined. The materials examined had a wide range of surface areas. Surface areas differed from product specifications, to varying degrees, and between products with similar dimensions and purity. The findings emphasize the multiple factors that can influence surface area and mark its utility for CNT characterization, a prerequisite to understanding their potential applications and toxicities. Implications for occupational monitoring are discussed.

EXPERIMENTAL

Materials

CNTs were obtained from the following sources: Nanostructured and Amorphous Materials Inc. (NanoAmor, Houston, TX, USA), Chengdu Organic Chemicals Co. Ltd Chinese Academy of Sciences (Timesnano, Chengdu, China), Mitsui & Co. Ltd (Mitsui, Tokyo, Japan), Carbon Nanotechnologies Inc. (CNI, Houston, TX, USA), and SouthWest NanoTechnologies Inc. (SWeNT, Norman, OK, USA). All samples were produced via chemical vapor deposition (CVD) except for the SWCNTs from CNI, which were produced by the HiPco® (high-pressure carbon monoxide) process. Two raw CNF products and a processed, purified final product obtained from a major producer (anonymous) also were examined. The raw CNF products were treated at high temperature in an inert gas to remove any associated organic compounds and catalyst residue. For the purpose of quality assurance, a carbonaceous

material (ASTM D24 SRB B-8 carbon black) with known surface area was included in the sample set. The material was purchased from Laboratory Standards and Technologies (Borger, TX, USA).

BET surface area measurement

The BET surface area analysis was performed with either a Micromeritics Gemini 2375 instrument (Laboratory 1) or a Micromeritics TriStarII 3020 instrument (Laboratory 2). Sample mass was typically 200 mg or more, with a minimum of 100 mg. All samples were degassed in ultra-high purity (UHP) nitrogen for 30 min at 90°C and then for 90 min at 200°C. The free space was measured using UHP helium gas. The SSAs were determined by a 5-point BET measurement with UHP nitrogen as the adsorbate and liquid nitrogen as the cryogen. The following relative pressures (P/P0) were used: 0.05, 0.10, 0.15, 0.2, and 0.25. A 50-point nitrogen isotherm analysis also was performed on two samples to determine BET surface area (and average pore size and single-point total pore volume at a P/P0 = 0.99).

Analytical precision, with this specific equipment and samples of relatively high surface area, was reported by the laboratory at ±5%. As part of the quality assurance procedures, repeat analyses were performed and some samples were analyzed by two different laboratories. To examine the possible influence of degassing temperature, several samples were reanalyzed by the same method, except with preheating at 100 or 300°C rather than 200°C. Details and results of these procedures are provided as Supplementary material (available at *Annals of Occupational Hygiene* online).

SEM with EDS

Analysis by SEM/EDS provided elemental and overall morphological information. Full details of the analysis and an in-depth discussion of the results will be given elsewhere. A brief description is included here to provide supporting data for the conclusions drawn regarding the surface area results.

Samples were prepared for SEM analysis by dispersion in amyl acetate (≥99%, CAS No. 628-63-7; Sigma-Aldrich, Milwaukee, WI, USA). A tungsten needle was used to transfer a small amount of the dispersed material to a beryllium substrate. The samples were imaged uncoated. Analysis of the first sample (Sample 4) was performed on a JEOL JSM-6480LV SEM (resolution 3.5 nm) using a working distance of 10 mm and accelerating voltage of 10 kV for imaging and 30 kV for EDS. All other samples were analyzed on a JEOL JSM-6480LX SEM, again with an accelerating voltage of 10 kV for imaging and 30 kV for EDS. EDS spectra (elemental analysis) were acquired using an Oxford INCA microanalysis system with a 50-mm^2 silicon drift detector. Images were taken from three representative areas and spectra of the same areas were acquired.

TEM with EDS

Analysis by TEM/EDS provides structural, morphological, and elemental information. As with the SEM/EDS results, details of the analysis and a full discussion of the results will be provided elsewhere. A brief description is given here to provide supporting data for conclusions regarding the surface area results.

All samples were analyzed on a JEOL JEM-3010 TEM operated at 300 kV. Elemental analysis was performed with an Oxford INCA EDS system with an atmospheric thin window detector (elements down to boron), mapping capability, spectrum imaging, and drift collection software. Except for one sample (Sample 4), samples were prepared by placing a small amount of material in a 1.5-ml centrifuge tube with approximately 1 ml of isopropyl alcohol (≥99.9%, CAS No. 67-63-0, high-performance liquid chromatography grade; Fisher Scientific). Samples were sonicated in an ultrasonic bath for at least 5 min; several required a longer sonication period (up to 15 min) for dispersion. In a few instances, the suspension appeared too concentrated and was diluted (to avoid overloading). After dispersion, a drop of the suspension was applied to a holey carbon-coated TEM grid (200 mesh; SPI Supplies, West Chester, PA, USA) and allowed to dry. No discernible settling of the material occurred prior to application of the suspensions. Distilled water was used for Sample 4 because it provided better dispersion of the material.

Thermogravimetric analysis

TGA was performed on the samples to investigate their residual ash content. All samples were analyzed on a Q5000IR TGA (TA Instruments Inc., New Castle, Delaware, USA). The initial sample weight ranged from 5 to 15 mg, except three CNF samples, which ranged from 1 to 5 mg, due to the 'fluffy' structure. Two methods were utilized to determine residual ash content, both of which were expected to provide similar results for residual ash. The different methods used

relate to another project; the results for the two methods were averaged, with standard deviations reported. Because complete oxidation occurred with both methods, results were equivalent and thus averaged. The first method was comparable to NIOSH 5040 (Birch, 2003), starting at room temperature then increasing by 50°C per minute to 850°C in nitrogen. The sample oven was held at 850°C for 2 min and then cooled to 500°C. The gas was switched to air, and the temperature was then increased at 50°C per minute to 920°C and held at 920°C for 2 min. The second method was performed in air, ramping from room temperature to 920°C at 5°C per minute. For all samples, mass loss rates near the end of the analysis were near zero.

Inductively coupled plasma atomic emission spectroscopy

The metal contents of the samples were examined by ICP-AES (Spectro Modula EOP; Spectro Analytical Instruments Inc., Mahwah, NJ, USA). Samples were placed into pre-weighed capped glass vials and weighed. They were then transferred to 125-ml beakers in a fume hood for digestion and analysis according to NIOSH Method 7300, modified for bulk CNTs. Specifically, for sample digestion, 5 ml of concentrated nitric acid and 20 ml of concentrated perchloric acid were added to each sample. The samples were covered with a watch glass and refluxed at 200°C until dissolution occurred. The watch glass covers were then removed and the samples were heated at 150°C until they had reached near dryness. The residues were dissolved in a dilute solution (4/1%) of nitric acid/perchloric acid (10 ml final volume) and analyzed for trace metals by ICP-AES. The samples were filtered with 0.45-µm filters prior to analysis, if needed. Samples were analyzed for the following metals: Ag, Al, As, Ba, Be, Ca, Cd, Co, Cr, Cu, Fe, K, La, Li, Mg, Mn, Mo, Na, Ni, P, Pb, Sb, Se, Sr, Te, Ti, Tl, V, Y, Zn, and Zr. Analysis of Mo, Na, Sb, Te, Ti, and Zr are considered semiquantitative because the standard solutions used to check recovery lacked these six elements. Analytical precision (RSD) for the ICP-AES instrument ranges from ~0.5 to 3%.

RESULTS AND DISCUSSION

Quality assurance

All repeat BET analyses showed good agreement (see Supplementary Tables S1 and S4, available at *Annals of Occupational Hygiene* online). Analytical precision for repeat analyses, at the same or at two different laboratories, was better than 4% (Supplementary Table S1, available at *Annals of Occupational Hygiene* online). Correlation coefficients (r^2) for BET fits were typically 0.9999 or better, with no value <0.9998. For the two laboratories, the mean result (n = 3, RSD = 1%) for the ASTM material (ASTM D24 SRB B-8 carbon black) was 140.7 m^2g^{-1}, which is within ~1% of the reported value (142.6 m^2g^{-1}).

Full results and details regarding the BET analyses and quality assurance measures are provided as Supplementary material (available at *Annals of Occupational Hygiene* online). In brief, heating the samples at 300°C and 200°C for 90 min gave comparable results (Supplementary Table S2, available at *Annals of Occupational Hygiene* online), as did 5-point BET and 50-point isotherm analyses (Supplementary Table S3, available at *Annals of Occupational Hygiene* online). Sample preparation at 100°C gave lower (some slightly) surface areas than at 200°C (Supplementary Table S4, available at *Annals of Occupational Hygiene* online), which is attributed to incomplete pore clearing of condensates. Degassing was, therefore, performed at 200°C to remove adsorbed compounds.

Influence of CNT properties on BET surface area

The varying properties of CNTs can result in widely different surface areas. For CNTs, the number of walls, tube diameter, surface functionalization, and metal and amorphous carbon impurities are important contributors to varying surface area (Peigney *et al.*, 2001; Chakraborty *et al.*, 2006; Naseh *et al.*, 2009). Length is an additional variable explored in this paper. Sonication, which promotes debundling of fibers, was reported to increase surface area (Peigney *et al.*, 2001), but this parameter was not addressed. The method of synthesis also may influence surface area, especially because of differences in the purity of the products, but this specific parameter also was not evaluated.

Before further discussion of the properties that influence SSA, it is helpful to briefly discuss nitrogen adsorption on CNTs. Nitrogen may adsorb to multiple surfaces of the typically bundled CNTs (Peigney *et al.*, 2001; Kondratyuk and Yates, 2007). Externally, nitrogen may adsorb to the outer surface of the curved portion of a CNT or in a groove site, which is the groove formed by two adjacent CNTs in a bundle. Nitrogen can also

adsorb to the inner core of a CNT, if accessible, and the interstitial space between three or more CNTs in a bundle (Agnihotri *et al.*, 2005; Byl *et al.*, 2005). Nitrogen has a kinetic diameter of 3.64 Å (Reid and Thomas, 1999), allowing the nitrogen adsorption to occur both outside and inside the CNTs, except for the spaces between the layers of MWCNTs, which are reported to be approximately 3.4 Å apart (Endo *et al.*, 2004). Whether the tubes are open or closed when comparing BET SSA values is an important consideration. Some authors make the assumption that the tubes are all open, while others assume they are closed. However, the production process (synthesis, purification, and functionalization) determines whether the CNTs are open or closed (Mackie *et al.*, 1997; Peigney *et al.*, 2001; Du *et al.*, 2002; Endo *et al.*, 2004; Li *et al.*, 2004; Agnihotri *et al.*, 2005; Byl *et al.*, 2005). Typically, CNTs are closed on the ends until they undergo various treatments for purification and/or functionalization, which can open the ends of the CNTs to varying degrees.

Theoretical calculations of the surface area of CNTs have been performed. Maximizing the surface area of SWCNTs is a goal for multiple applications such as catalyst development and gas storage; therefore, the majority of theoretical calculations are done for SWCNTs to estimate maximum values. Yin *et al.* (1999) determined the theoretical estimates via Monte Carlo simulation, assuming a square array for SWCNTs with diameters of 3 nm, 0.4 nm spacing, and open tube ends, to be ~3200 m^2g^{-1}. This compares to ~1200 m^2g^{-1} for the same scenario with closed tubes. Peigney *et al.* (2001) performed theoretical calculations for individual SWCNTs and found the SSA to be 1315 m^2g^{-1} assuming all tubes are closed. The SSA was calculated to be 751 m^2g^{-1} for a bundle of seven SWCNTs in a triangular network. As for MWCNTs, Peigney *et al.* (2001) reported the SSAs for a range of individual MWCNTs: 50 m^2g^{-1} for a 35-nm diameter 40-walled tube; 175 m^2g^{-1} for a 15-nm diameter, 10-walled tube; and 500 m^2g^{-1} for a 6-nm diameter, 3-walled tube.

A wide range of SSA values for CNTs has been reported, with values depending on multiple factors such as synthesis procedure, purification methods, and chemical and physical properties. For MWCNTs, values from 22.38 (Zhu *et al.*, 2003) to 1670 m^2g^{-1} (Raymundo-Pinero *et al.*, 2005) have been reported. The low result for MWCNTs was attributed to the large amount of impurities (amorphous carbon particles, multi-layer polygonal particles, and large graphite platelets) found in the sample after carbon arc synthesis, while the high result is attributed to increased porosity due to chemical activation of a disordered MWCNT sample synthesized by CVD. SWCNTs have been found to have SSAs from 2 (Martinez *et al.*, 2003) to 1587 m^2g^{-1} (Cinke *et al.*, 2002; Li *et al.*, 2004; Hemraj-Benny *et al.*, 2008). The low surface area SWCNTs was produced via arc-discharge and originally had a SSA of 236 m^2g^{-1}. They were then acid treated and air oxidized, which reportedly introduced functional groups and intercalated acid molecules blocking the entry of the adsorbing gas, resulting in an extremely low SSA of 2 m^2g^{-1}. The high surface area of the SWCNTs is attributed to treating HiPco® SWCNTs with *N*,*N*-dimethylformamide/ethylene diamine to debundle the tubes, followed by acid treatment and oxidation to remove impurities and open the tubes. Overall, a wide range of SSA values has been reported for CNTs, but commonly reported values range from ~150 to 600 m^2g^{-1} for SWCNTs (Eswaramoorthy *et al.*, 1999; Fujiwara *et al.*, 2001; Cinke *et al.*, 2002; Martinez *et al.*, 2003; Kayiran *et al.*, 2004; Li *et al.*, 2004; Chakraborty *et al.*, 2006; Hemraj-Benny *et al.*, 2008) and from ~15 to 300 m^2g^{-1} for MWCNTs (Tsang *et al.*, 1993; Yin *et al.*, 1999; Raymundo-Pinero *et al.*, 2002; Zhu *et al.*, 2003; Li *et al.*, 2004; Chen and Wang, 2006; Zacharia *et al.*, 2007; Naseh *et al.*, 2009).

Results of BET measurements for materials examined in this study are summarized in Table 1. The ASTM standard, carbon black, which has a reported surface area of 142.6 m^2g^{-1}, was determined to have an average surface area of 140.7 m^2g^{-1} (RSD = 0.4%, n = 3), within ~1% of the reported value and well within the ±5% reported analytical error. The SSAs for the different CNT materials examined ranged from a low of 22 m^2g^{-1} for the Mitsui MWCNT (Sample 7) to a high of 662 m^2g^{-1} for a NanoAmor SWCNT (Sample 1). Excluding the Mitsui material and one Timesnano MWCNT (Sample 14) that underwent heat treatment at 2800°C, the range of SSAs is comparable to the range of values found in the literature. How measured results compare to vendor specifications, and how different properties may influence SSA are discussed in following sections.

Product comparison

Different manufacturers using CVD synthesis and offering CNT products with similar properties were examined. A SWCNT (Sample 1) from NanoAmor [1–2 nm outer diameter (OD); 5–30-µm length] had a SSA of 662 m^2g^{-1}, while a

Table 1. BET SSAs of commercially available carbon nanomaterials.

SN	Manufacturer, product	Production method	OD, nm	Length, μm	Purity	BET SSA, m^2g^{-1}	Manufacturer-listed SSA, m^2g^{-1}
1	NanoAmor, SWCNT	CVD	1–2	5–30	>90 v/v% SWCNTs >95 v/v% CNTs	662	~400
2	Timesnano, SWCNT	CVD	1–2	5–30	>90%	367	>380
3	CNI, SWCNT	HiPco®	1	0.3–1	>90%	144	NA
4	SWeNT, SWCNT	CoMoCAT®	0.9 ± 0.3	0.3–3	>90% by weight carbon content	616	NA
5	NanoAmor, MWCNT	CVD	10–20	10–30	>95%	146	200–350
6	Timesnano, MWCNT	CVD	10–20	10–30	>95%	177	>200
7	Mitsui, MWCNT	CVD	40–90	10–20	>95%	22	NA
8	Timesnano, SWCNT	CVD	1–2	5–30	>60%	392	>407
9	Timesnano, SWCNT	CVD	1–2	1–3	>90%	344	>380
10	Timesnano, SWCNT-COOH (2.73 wt%)	CVD	1–2	5–30	>90%	354	>380
11	Timesnano, SWCNT-OH (3.96 wt%)	CVD	1–2	5–30	>90%	310	>380
12	Timesnano, DWCNT	CVD	2–4	~50	>60%	384	>350
13	Timesnano, MWCNT	CVD	10–30	10–30	>85%	119	>200
14	Timesnano, MWCNT	CVD, 2800°C	10–20	10–30	>99.9%	74	>100
15	Timesnano, MWCNT	CVD	20–30	10–30	>95%	118	>110
16	Timesnano, MWCNT	CVD	10–20	0.5–2	>95%	180	>200
17	Timesnano, MWCNT-COOH (2.00 wt%)	CVD	10–20	10–30	>95%	171	>200
18	Timesnano, MWCNT-OH (3.06 wt%)	CVD	10–20	10–30	>95%	192	>200
19	CNF reactor 1	VGCF	70–200	50–200	NA	2.0	NA
20	CNF reactor 2	VGCF	70–200	50–200	NA	19	NA
21	CNF final product	VGCF	70–200	50–200	>99% fibrous material	35	20–30
22	SRB 8 ASTM black carbon	–	–	–	99% carbon by weight	141	142.6

NA, not available; OD, outer diameter as listed by manufacturer; SN, sample number; VGCF, vapor grown carbon fiber (patented process). Length and purity are as listed by manufacturer.

SWCNT from Timesnano with the same purity, OD, and length (Sample 2) had a SSA of 367 m^2g^{-1}. The SWCNTs from SWeNT (Sample 4), which have reported diameters that are slightly less (0.9 ± 0.2-nm OD) than the other two products, had a SSA of 616 m^2g^{-1}. The SWCNTs from CNI (Sample 3) had a SSA of 144 m^2g^{-1}, much lower than the other materials and the value reported by

the supplier. This CNI material was produced by the HiPco® process rather than CVD.

Differences exist in the residual ash content and total metal mass percentage (Table 2) between samples provided by different manufacturers. Sample 3, with the lowest SSA, has the highest residual ash content of any of the SWCNT samples (21.63 ± 3.42%). Sample 4 has the next highest ash of the SWCNTs, at 7.42 ± 0.11%, followed by Timesnano (Sample 2: 6.39 ± 0.16%) then NanoAmor (Sample 1: 2.39 ± 0.07%). The ICP-AES results for different manufacturers show a trend similar to the TGA results. Sample 3 has a total metal mass percentage of 13.3, Sample 4 has 5.13, Sample 2 has 3.63, and Sample 1 has a total metal mass percentage of 1.85, corresponding to their decreasing residual ash contents. A similar range for SWCNT metal content has been reported (Plata *et al.*, 2008).

MWCNTs (10–20-nm OD; 10–30-μm length) purchased from NanoAmor (Sample 5) had a measured SSA of 146 m^2g^{-1} (Table 1). A comparable MWCNT material from Timesnano (Sample 6) had a SSA of 177 m^2g^{-1}, while the Mitsui MWCNTs (Sample 7) had the lowest SSA of only 22 m^2g^{-1}. Differences between TGA results for different samples from different manufacturers were less for the MWCNT samples compared to SWCNTs, with the residual ash being 0.96 ± 0.20%, 0.79 ± 0.43%, and 0.36 ± 2.06% for Samples 5, 6, and 7, respectively. The ICP-AES results again follow the same trend between manufacturers as the TGA results, with total metal mass percentages being 0.78, 0.65, and 0.48 for Samples 5, 6, and 7, respectively.

Obviously, the SSAs of CNTs from different suppliers may exhibit a wide range of values (Table 1). Different processing methods utilized by different manufacturers influence important factors such as tube bundling, fraction of open tubes, and the amounts and types of impurities present, contributing to the varying SSAs of these materials. As indicated in Table 1, suppliers often report a range of SSAs for their CNT products; however, our results for these materials differ, to varying extents, from the reported values, sometimes substantially.

Table 2. Summary of TGA and ICP-AES results for commercially available carbon nanomaterials.

SN	Manufacturer, product	Residual ash, % (SD)	Total metal (mass %)
1	NanoAmor, SWCNT	2.39 (0.07%)	1.85
2	Timesnano, SWCNT	6.39 (0.16%)	3.63
3	CNI, SWCNT	21.63 (3.42%)	13.33
4	SWeNT, SWCNT	7.42 (0.11%)	5.13
5	NanoAmor, MWCNT	0.96 (0.20%)	0.78
6	Timesnano, MWCNT	0.79 (0.43%)	0.65
7	Mitsui, MWCNT	0.36 (2.06%)	0.48
8	Timesnano, SWCNT	5.05 (0.62%)	3.37
9	Timesnano, SWCNT	3.71 (0.11%)	1.67
10	Timesnano, SWCNT-COOH (2.73 wt%)	1.54 (0.27%)	1.06
11	Timesnano, SWCNT-OH (3.96 wt%)	3.15 (0.32%)	1.28
12	Timesnano, DWCNT	4.59 (0.18%)	2.98
13	Timesnano, MWCNT	9.73 (1.06%)	7.34
14	Timesnano, MWCNT	0.35 (0.30%)	0.27
15	Timesnano, MWCNT	2.6 (0.16%)	1.98
16	Timesnano, MWCNT	0.69 (0.11%)	0.73
17	Timesnano, MWCNT-COOH (2.00 wt%)	0.85 (0.39%)	0.61
18	Timesnano, MWCNT-OH (3.06 wt%)	1.14 (0.24%)	0.69
19	CNF reactor 1	0.59 (0.44%)	1.11
20	CNF reactor 2	1.2 (0.31%)	0.99
21	CNF final product	1.48 (0.60%)	1.15
22	ASTM black carbon	0.25 (0.34%)	0.12

SD, standard deviation; SN, sample number.

Measured versus supplier-listed SSAs are plotted in Fig. 1 for easy comparison.

Impurities

Increases in BET surface area have been seen after removal of amorphous carbon through thermal treatment and after acid treatment to remove metal impurities associated with CNTs (Eswaramoorthy *et al.*, 1999; Li *et al.*, 2003; Chen *et al.*, 2007). The increase is partially due to an increase in the surface accessible for nitrogen adsorption after removal of impurities. Eswaramoorthy *et al.* (1999) reported SWCNTs with a surface area 376 m^2g^{-1}, increasing to 483 m^2g^{-1} after hydrochloric acid treatment, which opens the CNT hollow core known as a pore. After nitric acid treatment, which opens pores and eliminates carbon impurities, surface area increased to 429 m^2g^{-1}. Cinke *et al.* (2002) studied a HiPco® material before and after iron impurities had been removed, and debundling via dimethylformamide/ethylene diamine treatment had been performed, and found that the surface area drastically increased from 577 to 1587 m^2g^{-1}. Li *et al.* (2004) found pure synthesized SWCNTs to have a surface area of 619.1 m^2g^{-1}; addition of MWCNT impurity to the sample decreased the surface area to 396.5 m^2g^{-1}, with 47.9% SWCNT still present. Ning *et al.* (2005) concluded that BET surface area measurements were an efficient way to determine purity during the synthesis of SWCNTs, with higher purity samples having higher surface areas. Chen *et al.* (2007) reported an increase in surface area for MWCNTs synthesized by CVD, from 133.66 to 167.92 m^2g^{-1} for 10–20-nm OD MWCNTs after an acid microwave treatment for purification. Overall, for both SWCNTs and MWCNTs, an increase in purity is expected to correlate with an increase in surface area.

A special case to consider is highly graphitized CNTs. Graphitization of MWCNTs (typically at a temperature upwards of 2000°C) increases the purity and uniformity in MWCNTs and decreases the amount of metal catalyst impurity in the CNTs (Andrews *et al.*, 2001; Delpeux-Ouldriane *et al.*, 2006). Although graphitization is associated with processes that may lead to an increase in surface area, typically the surface area decreases after graphitization. Delpeux-Ouldriane *et al.* (2006) and Andrews *et al.* (2001) pointed out that graphitization causes more ordering of the walls of

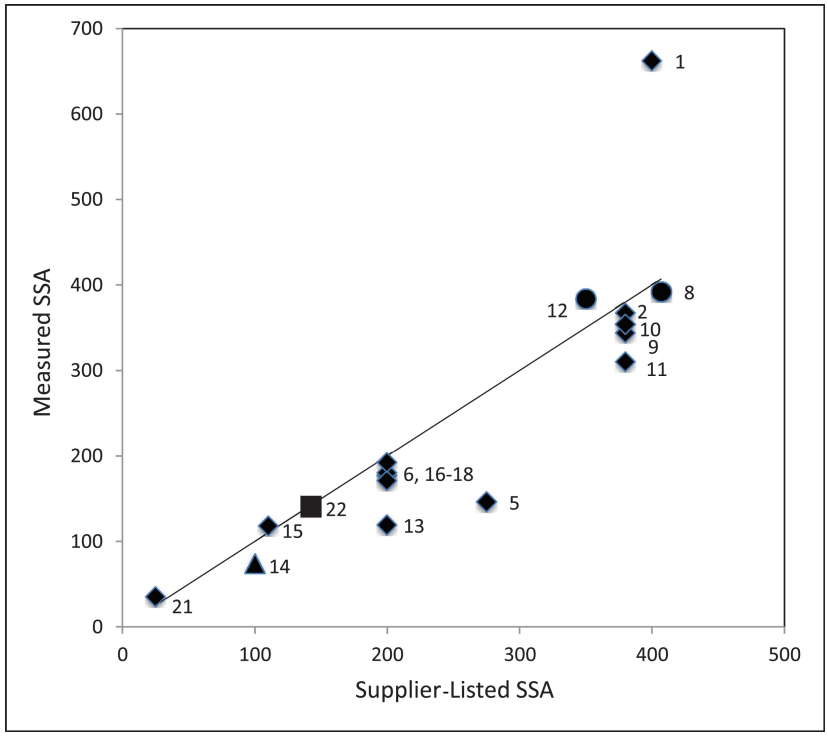

Fig. 1. Measured versus supplier-listed SSAs of CNTs and CNFs. Circle markers correspond to lowest purity (>60%) CNTs, the triangle marker is highest purity (>99%) CNT, and the square marker is ASTM carbon black. Marker numbers correspond to sample numbers in Table 1. Solid line is expected trend (unity slope).

MWCNTs, leading to removal of microstructural defects, and closing of MWCNT ends. Overall, a decrease of sidewall microstructural defects leading to decreased accessibility of the inner nanotubes, as well as closing of the CNT ends, is likely the reason for the decrease in the SSAs for graphitized samples.

Results for two Timesnano SWCNTs (1–2-nm OD; 5–30-μm length) having purities of >90% (Sample 2) and >60% (Sample 8) show an increase in surface area for the lower purity product, from 367 to 392 m^2g^{-1}, which is not expected based on most literature reports (Eswaramoorthy *et al.*, 1999; Li *et al.*, 2003; Chen *et al.*, 2007). The SSAs for both materials are lower than those reported by the supplier, >380 m^2g^{-1} for high-purity SWCNTs and >407 m^2g^{-1} for low-purity SWCNTs, but the relative results are consistent. However, the literature mentions problems with purification of CVD-produced SWCNTs, especially on a large scale. The oxidation treatments utilized to purify SWCNTs can cause the following: (i) oxidation of the SWCNTs, which leads to open pores being blocked; (ii) damage and distortion of the SWCNTs; and (iii) damage to the SWCNTs due to removal of metal impurities inside of the SWCNTs (Montoro and Rosolen, 2004; Park *et al.*, 2006). Damage to the surface of the nanotubes generates carbonaceous impurities such as amorphous carbon, fullerenes, graphitic particles, and carbon shells. Sample 8 does have slightly less residual ash content and less total metals than Sample 2, based on the TGA and ICP-AES results (Table 2). Therefore, blocked pores may be the main contributor to the decrease in SSA. Although the manufacturer lists a higher purity for Sample 2 than Sample 8, either because of fewer metals or more SWCNTs present, the SSA may have decreased because of the purification treatment. The 7.4% ash content of SWCNT Sample 4 (SWeNT), yet relatively high SSA of 616 m^2g^{-1}, seems counter to the trend of higher SSA for higher purity materials. However, this particular material was produced with a high surface area catalyst; catalyst impurities may have increased SSA. Further, synthesis was by CO disproportionation in a unique CoMoCAT® process that produces SWCNTs with smaller diameters (1 nm and less) and a narrower diameter distribution relative to other CVD methods, which also may explain the relatively high SSA. Measured diameters (Table 3) were <1 nm, while comparable materials had diameters ranging from 1 to 5 nm.

Table 3. Summary of SEM and TEM results for commercially available carbon nanomaterials.

SN	Manufacturer, product	MOD, nm	EOD, nm	Other diameters experimentally observed	Other features observed experimentally
1	NanoAmor, SWCNT	1–2	2–5	Some 20–60-nm CNTs	MWCNTs present; some CNTs had a nodular structure (i.e. nodes along length)
2	Timesnano, SWCNT	1–2	1–3		Mainly SWCNT bundles or ropes; MWCNTs present, some with nodular structure
3	CNI, SWCNT		1–2		Continuous CNT networks of long bundles or ropes of variable diameter
4	SWeNT, SWCNT	0.9 ± 0.2	0.6–0.7		Many nanoropes with 5–15-nm ODs, some with larger diameters and/or nodular structures; SWCNT bundles; rolled/folded graphite sheets
5	NanoAmor, MWCNT	10–20	10–20	Some 20–40-nm CNTs	
6	Timesnano, MWCNT	10–20	10–20	Some 20–70-nm CNTs	
7	Mitsui, MWCNT	40–90	45–85	Some 150–250 nm and some 10–15-nm CNTs	Long, smooth CNTs with hollow cores and clusters of nodular structures
8	Timesnano, SWCNT	1–2	1–2		Many CNTs with nodular structure
9	Timesnano, SWCNT	1–2	1–2		Similar to Sample 8; many MWCNTs with nodular structures and one atypical sheet-like graphite structure
10	Timesnano, SWCNT-COOH (2.73 wt%)	1–2	1–2		Similar to Samples 8 and 9
11	Timesnano, SWCNT-OH (3.96 wt%)	1–2	1–2		Similar to Samples 8, 9, and 10; also observed sheet-like graphitic structure

Table 3. *Continued*

SN	Manufacturer, product	MOD, nm	EOD, nm	Other diameters experimentally observed	Other features observed experimentally
12	Timesnano, DWCNT	2–4	4–5		Mixture of smooth-walled CNTs with continuous hollow cores (mainly bundles and ropes of DW, SW, and MW CNTs); MWCNTs with nodular and internally segmented structures
13	Timesnano, MWCNT	10–30	10–30	Some 50–60-nm CNTs	MWCNTs had a nodular and an internally segmented structures
14	Timesnano, MWCNT	10–20	10–20		Some long MWCNTs (100–200 μm long with 5–10 nm diameters) tapering to points at each end; MWCNTs with nodular or segmented structures; tubes not fully graphitized
15	Timesnano, MWCNT	20–30	15–30	Some from 9–70 nm	
16	Timesnano, MWCNT	10–20	10–20	Some from 7–60 nm	
17	Timesnano, MWCNT-COOH (2.00 wt%)	10–20	10–20	Some from 20–35 nm	Large, irregularly shaped carbonaceous particles in some areas
18	Timesnano, MWCNT-OH (3.06 wt%)	10–20	10–20	Some from 20–50 nm	
19	CNF reactor 1	70–200	50–70	35–140-nm smooth-walled and 35–80-nm segmented fibers; aggregates of spherical particles 250 nm in diameter	Mix of spherical particles and long CNFs; CNFs had either smooth walls and hollow cores or nodular walls and an internally segmented structure; CNFs were multi-walled and not fully graphitized; TEM showed many areas of turbostratic (disordered) layering; larger diameter fibers seen at low magnification, but these did not show highly ordered layers at high magnification
20	CNF reactor 2	70–200	50–80	Spherical particles 250–500 nm; smooth segmented fibers 50–150 nm	Same as Sample 19
21	CNF final product	70–200	50–80	Spherical particles 250–500 nm; fibers with diameters 160–225 nm; smooth segmented fibers 50–150 nm and 160–225 nm	Same as Sample 19
22	ASTM black carbon	NA	5–50		Aciniform (grape-like) clusters of roughly spherical primary particles; disordered graphitic layers present

EOD, experimentally determined outer diameter (majority observed); MOD, manufacturer-listed outer diameter; SN, sample number.

In addition to metal impurities, TEM and SEM analyses indicate that all SWCNT samples contain MWCNTs, with the exception of the CNI SWCNT (Sample 3), which appeared to be almost exclusively SWCNTs. Other carbon impurities also were found in some of the samples. The short Timesnano SWCNTs (Sample 9) showed one atypical sheet-like graphitic structure (Fig. 2). The Timesnano SWCNT-OH sample (Sample 11) also contained sheet-like graphitic structures.

Industrial-grade (purity >85%) MWCNTs (Sample 13) did exhibit a lower surface area, 119 m^2g^{-1} compared to 177 m^2g^{-1} for a higher purity MWCNTs (Sample 6), as expected. This is typically due to the increased metal and amorphous carbon impurities. The TEM results show that both samples have some CNTs with larger diameters, but more importantly, Sample 13 also contains MWCNTs with internally segmented structures, which would lead to a decrease in SSA

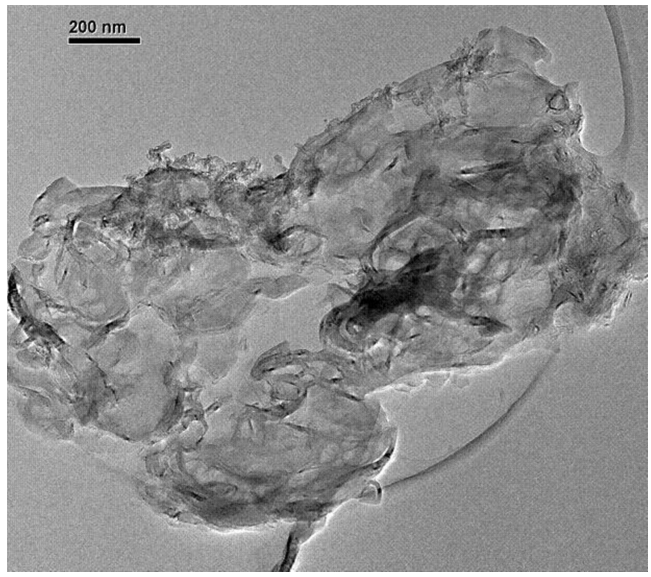

Fig. 2. TEM image of short Timesnano MWCNTs, Sample 9, showing atypical sheet-like graphitic structure.

due to the inaccessible inner surface of the CNTs. As can be seen in Fig. 3, Sample 13 contains many more impurities compared to Sample 6. The TGA and ICP-AES results both support these conclusions, as the residual ash content and total metals present are both significantly larger for the lower purity sample. The highly graphitized MWCNTs (Sample 14), with equivalent diameter and length ranges, had an SSA of 74 m^2g^{-1}, consistent with the decreased SSAs reported for these (graphitized) materials. Also, Sample 14 had lower residual ash and total metal contents, as seen from the TGA and ICP-AES data. The SEM/EDS and TEM/EDS results were quite consistent between the samples, showing carbon, oxygen, silicon, and sulfur as the only elements present besides the iron catalyst particles (Table 4). Minor differences were observed as aluminum was found in only one area of Sample 19, titanium was found in one region of Sample 19, and calcium was found in only one region of Sample 20. These results likely reflect sample inhomogeneity and the limited area/volume analyzed.

SEM and TEM analyses revealed interesting morphological features in some MWCNT samples. For example, the Timesnano double-walled CNTs (DWCNTs; Sample 12) had a mixture of smooth-walled nanotubes with continuous hollow cores that were mainly bundles and ropes as well as some DWCNTs, SWCNTs, and MWCNTs individually seen. Also present were nanotubes that were not smooth on the surface but rather had the appearance of nodules and chain-like segments (Fig. 4). Highly graphitized nanotubes from Timesnano (Sample 14) had large elongated particles present (100–200 µm long and 5–10 nm diameters) tapering to points/caps at each end. Sample 14 also contained MWCNTs with nodular or segmented morphologies that were not fully graphitized, which was recognized by their d-spacing (distance between layers) being 0.38–0.39 nm (as opposed to 0.335 for graphite). Refer to Table 3 for additional details.

Number of walls/diameter and length

Theoretical calculations of surface area indicate that surface area varies with the number of shells (walls) and diameter of CNTs (Peigney *et al.*, 2001), with the number of shells having a dominant influence on surface area over the diameter. The addition of a shell has a more dramatic influence because of the increased mass it contributes rather than surface area. Surface area is known to increase with decreasing outer diameter of CNTs (Peigney *et al.*, 2001; Chen *et al.*, 2007). As reported previously, length had no apparent influence on surface area (Chakraborty *et al.*, 2006).

Regarding results presented in this paper, the surface area of MWCNTs from Timesnano differed relative to outer diameter, with 10–20-nm OD tubes (Sample 6) having a SSA of 177 m^2g^{-1} and 20–30-nm OD tubes (Sample 15) having a SSA of 118 m^2g^{-1}. The SWCNTs (Sample 2), which have much smaller ODs (1–2 nm) than MWCNTs, have a higher surface area, 367 m^2g^{-1}, than MWCNTs.

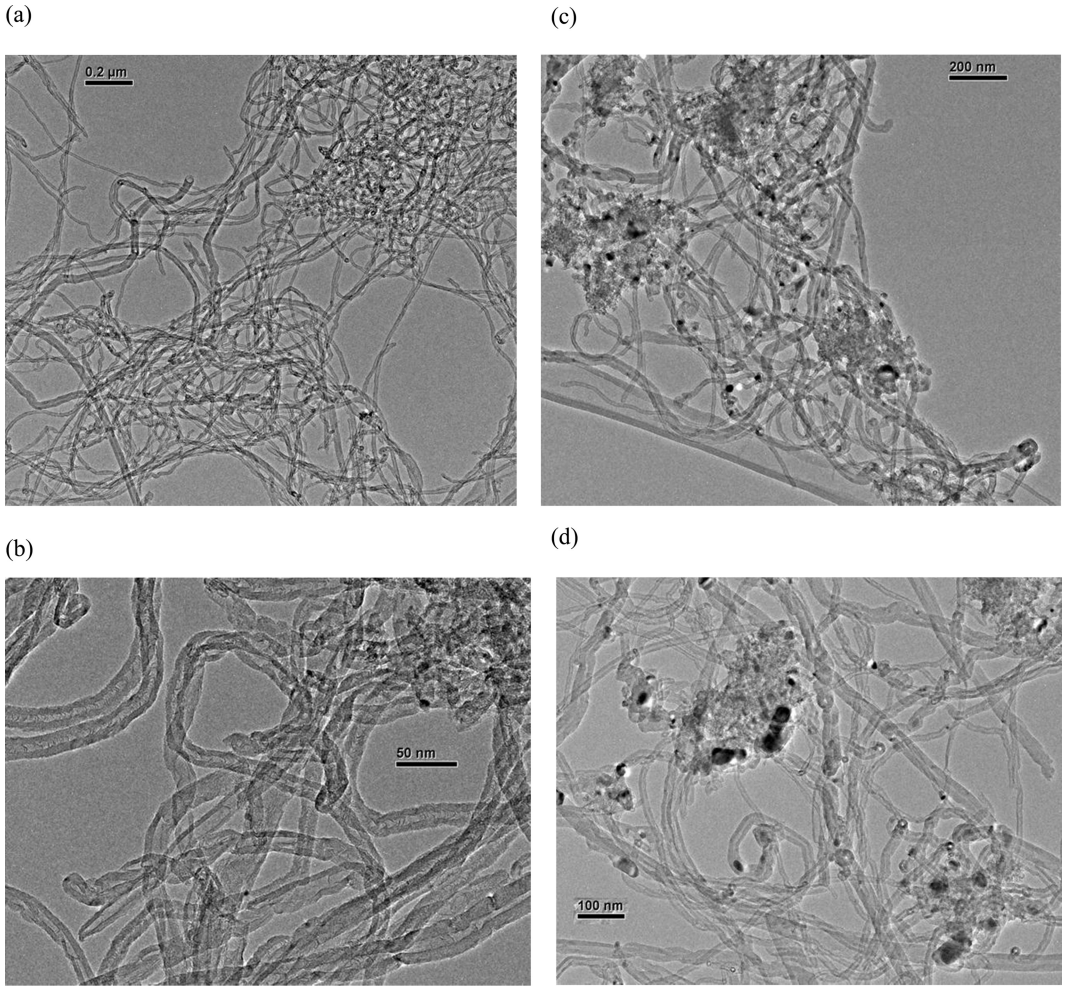

Fig. 3. TEM images of higher purity MWCNTs, Sample 6 (a and b) and lower purity MWCNTs, Sample 13 (c and d). Note that Sample 13 shows MWCNTs with impurities of amorphous carbon and metals.

A DWCNT from Timesnano (2–4-nm OD; 50-µm length) had a SSA of 384 m^2g^{-1} (Sample 12), similar to that of SWCNTs. The TEM results support our conclusion by showing good agreement between the supplier-listed diameters and the experimentally determined diameters. The CNT impurities (i.e. non-MWCNT CNT) found in Sample 15 had diameters of 9–70 nm, while the CNT impurities in Sample 6 had diameters of 10–40 nm. Therefore, because the larger diameter MWCNTs (Sample 15) contain CNT impurities with diameters comparable to (or slightly larger than) the CNT impurities in the smaller diameter product (Sample 6), the impurities do not complicate the relationship of smaller diameter CNT samples having larger surface areas. Overall, our results for SSAs agree with the trends reported in the literature for number of walls and diameters of CNTs.

CNFs from a major manufacturer also were analyzed. Three samples were examined: two raw materials from two different reactors (Samples 19 and 20) and a final, processed product (Sample 21). The CNFs analyzed have an OD in the range of ~50–200 nm, significantly larger than that of the MWCNTs, and exhibited much smaller surface areas than most of the CNTs. The two raw products (Samples 19 and 20) have SSAs of 2 and 19 m^2g^{-1}, respectively, while the SSA of the final (Sample 21), processed product is 35 m^2g^{-1}. As determined by TEM analysis (Table 3), the diameters of the nanofibers from reactor 1 (Sample 19) ranged mainly from 50–70 nm, similar to those from reactor 2 (Sample 20), which were mainly 50–80 nm.

Table 4. Summary of SEM/EDS and TEM/EDS elemental analysis results for commercially available carbon nanomaterials. Carbon and oxygen were found in all samples and therefore omitted from the table for brevity. Corresponding CNT diameters and lengths are provided in Table 1.

SN	Manufacturer, product	SEM/EDS	TEM/EDS	Catalyst
1	NanoAmor, SWCNT	Co, Fe	Co, Fe	Co 2–5 nm; larger CNTs were associated with Fe
2	Timesnano, SWCNT	Minor Zn, Cl, S, Si, Mg, Al; trace Fe	Minor Zn, Cl, S, Si, Mg, Al	Co; also observed structures rich in Ca and F
3	CNI, SWCNT	Fe, Si; trace Ti, Cr	Fe, Si; trace S	Fe (particles closely packed and not individually observed)
4	SWeNT, SWCNT	Minor to trace Mo, Co; trace Na, Al, Si, Cl, Ca, Fe, Cu	C, O; minor to trace Mo, Co; trace Na, Al, Si, Cl, Ca, Fe, Cu	Co and Mo in varying ratios, 1–3-nm particles
5	NanoAmor, MWCNT	Ni, S, Si (Fe seen in one area)	Ca, K, Zn, Cl	Ni (SEM showed Ni with trace Fe)
6	Timesnano, MWCNT	Ni, Fe, S, Si	Ca, K, Cl	Ni (no Fe)
7	Mitsui, MWCNT	Si, S; trace Fe	Si, S	None found
8	Timesnano, SWCNT	Cl, S, Si, Mg, Ca, Fe, Co	Fe, Co	Co and Fe in varying ratios with significantly less Fe
9	Timesnano, SWCNT	Cl, S, Si, Ca, Ti, Fe, Co, Mb, Cr	Cl, S, Si, Ca, Ti, Fe, Co, Mb, Cr	Fe, Co, Mb, Cr in varying ratios
10	Timesnano, SWCNT-COOH (2.73 wt%)	S, Si, Ca, Co, Fe	S, Si, Ca, Co, Fe, Cl, Zn	Co, trace Fe; one large catalyst particle had Co, Fe, and Ni, Cr, Mn, V
11	Timesnano, SWCNT-OH (3.96 wt%)	Fe, Cr, Co, Mn, Si, S, Ca, Al	Ni, Fe, Cr, Co, Mn	Ni and Fe, Cr, Co, Mn in varied combinations and ratios
12	Timesnano, DWCNT	S (minor to trace Fe, Cr, Si, Mg, Cl, Ca, K, Na)	Co, Mb, Cu	Co and small amount of Mb; one particle also contained Ni
13	Timesnano, MWCNT	Ni, Al, Si, S, Ca, Cl, trace Fe	Ni, Al, Si, S, Ca, Cl	Ni
14	Timesnano, MWCNT	S, Si (trace Fe)	S, Si	None found
15	Timesnano, MWCNT	Ni, Fe, S, Si; Al and Cr in one area	Ni, Fe, Si (trace Cl in one location)	Ni and Fe in varying ratios (catalyst and aggregates)
16	Timesnano, MWCNT	Ni, Fe, S, Si, Ca	Ni, Si, Ca	Ni (catalyst and aggregates; no Fe)
17	Timesnano, MWCNT-COOH (2.00 wt%)	Ni, Fe, S, Si, Ca	Ni, Si, Ca, S, Cl, P	Ni (catalyst and aggregates; no Fe)
18	Timesnano, MWCNT-OH (3.06 wt%)	Ni, Fe, S, Si, Ca	Ni, Fe, Co, Si, S, Ca, Cl (trace Mn in one area)	Ni (catalyst and aggregate); Fe and Ni found in one catalyst particle; Ni and Co found in another catalyst particle
19	CNF reactor 1	Fe, Si, S, Al in one area	Fe, Si, S	Fe
20	CNF reactor 2	Fe, Si, S, Ti in one area	Fe, Si, S	Fe seen in the center of many spheres
21	CNF final product	Fe, Si, S	Fe, Si, S, Ca in one area	Fe
22	ASTM black carbon	Si, S, trace Fe, and Cl in one area	Si, S	

SN, sample number.

The final product (Sample 21) consisted of fibers mainly in the diameter range 50–80 nm. The SEM and TEM images of Samples 19–21 showed other structures as described in Table 3. Overall, Samples 19–21 were heterogeneous mixtures of spherical particles and long nanofibers. It also was noted for Samples 19–21 that some of the CNFs had an internally segmented structure and much

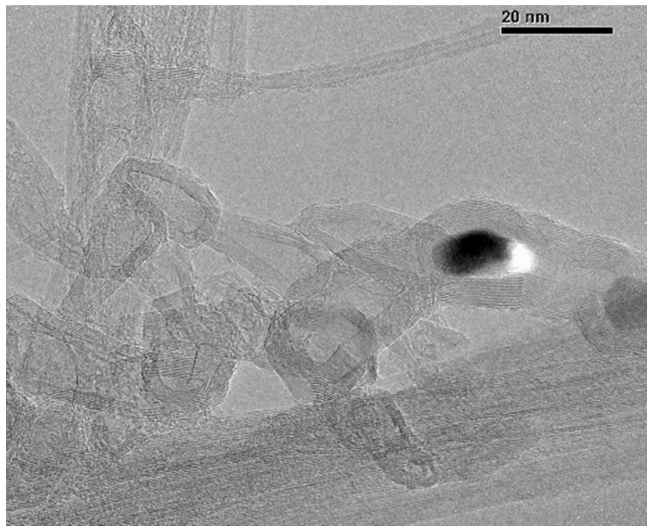

Fig. 4. TEM image of Timesnano DWCNTs, Sample 12, showing nanotubes with the appearance of nodules and segmented structure.

of the sample appeared to be turbostratic, which would prevent nitrogen adsorption in the core of the CNFs. The TGA results for Samples 19–21 showed residual ash contents of $0.59 \pm 0.44\%$, $1.2 \pm 0.31\%$, and $1.48 \pm 0.60\%$, respectively. The ICP-AES results followed a similar trend, when taking into account the standard deviations of the TGA results, in that the total metal mass percentages were similar, being 1.11, 0.99, and 1.15, respectively. The relationship between the diameter of the CNFs discussed here and SSA is not straightforward. It seems that multiple parameters (e.g. impurities, morphology, and structure) play a role for these particular products.

The SSA for a Timesnano SWCNT product (Sample 2) with a reported length of 5–30 μm was 367 m^2g^{-1}, which is slightly higher than the result of 343 m^2g^{-1} for a shorter (1–3 μm) material (Sample 9) purchased from this company. Surface area showed no significant difference when length varied from 10–30 μm (Sample 6), with a SSA of 177 m^2g^{-1}, and 0.5–2 μm (Sample 16), with a SSA of 180 m^2g^{-1}.

Functionalization with –OH and –COOH groups

Functionalization of CNTs may occur through a variety of treatments, which are detailed in the Supplementary material, available at *Annals of Occupational Hygiene* online. Naseh *et al.* (2009) have shown that both chemical and plasma functionalization of MWCNTs increase the SSA of the MWCNTs. Rationale provided indicates that the functionalization process opens tube ends and generates sidewall defects. These extra openings provide accessibility into the cavity of the CNTs, hence increasing SSA. Furthermore, functionalization of CNTs disturbs the π-π interaction between the tubes, causing debundling and increased SSA. Tube opening and removal of impurities (see Impurities section) during oxidative treatments also have been reported by others to explain the increase in SSAs. Specific examples are discussed in the Supplementary material, available at *Annals of Occupational Hygiene* online (Li *et al.*, 2003; Ye *et al.*, 2005; Chen and Wang, 2006). In general, an increase in SSA has been found when MWCNTs are oxidized (Li *et al.*, 2003; Ye *et al.*, 2005; Chen and Wang, 2006; Naseh *et al.*, 2009).

A decrease in SWCNT SSA has been reported after some specific functionalization reactions; examples are discussed in the Supplementary material, available at *Annals of Occupational Hygiene* online. In one study, a decrease in the SSA of HiPco® synthesized SWCNTs after ozonolysis was suggested to be due to rebundling of the SWCNTs (Chakraborty *et al.* 2006). An increase in SSA was then seen when these functionalized CNTs were reacted with acid and baked at high temperatures (Chakraborty *et al.*, 2006). Hemraj-Benny *et al.* (2008) saw a decrease in the SSA of SWCNTs after ozone treatment, and attributed it to functional groups blocking pore entrances and bundling of oxidized nanotubes via hydrogen bonding, which also blocks pore

entrances. Following ozone treatment, a hydrogen peroxide treatment was given, which still showed an overall decrease in SSA. The overall decrease was attributed to openings being blocked by surface functional groups, although there are more openings in SWCNTs due to the extensive oxidation treatments.

The severity of oxidative treatments may influence the SSA. It is possible that more mild treatments, such as an air oxidation, create openings that are essentially bored into the sidewalls of CNTs without formation of functional groups that may block the openings, therefore allowing for an increase in SSA (examples provided in the Supplementary material, available at *Annals of Occupational Hygiene* online). In general, the literature shows a decrease in SSA when SWCNTs undergo oxidative treatments (Martinez *et al.*, 2003; Byl *et al.*, 2005; Chakraborty *et al.*, 2006; Hemraj-Benny *et al.*, 2008).

The SSA results presented here are for –COOH- and –OH-functionalized SWCNTs and MWCNTs, though it is possible that functional groups other than those specified by the manufacturer are present. With both CNT types, –COOH functionalization created no significant change in SSA. Unfunctionalized SWCNTs from Timesnano (Sample 2) had an SSA of 367 m^2g^{-1}, similar to the SSA for carboxyl-functionalized (–COOH) SWCNTs (Sample 10), 353 m^2g^{-1}. Surface functionalization with –COOH (Sample 17) produced no significant difference relative to unfunctionalized MWCNTs (Sample 6), 171 m^2g^{-1} and 177 m^2g^{-1}, respectively. One explanation may be that the unfunctionalized materials had been processed via acid and heat treatments to obtain a highly purified sample, removing metals and possibly opening nanotubes. As noted (see Impurities section), purification can change the SSA; therefore, when comparing a purified sample with a surface functionalized sample, one may not expect to see a difference in the SSA because of the similar treatments.

After –OH functionalization, MWCNTs showed an increase in SSA, from 177 to 192 m^2g^{-1} (Table 1; Samples 6 and 18). This may be the result of a strong oxidation treatment that opened up the nanotubes significantly and caused tube debundling. Figure 5 shows TEM images of Samples 6 and 18. Sample 18 shows more open-ended MWCNTs than Sample 6. In contrast, an –OH-functionalized, SWCNT product (Sample 11) showed decreased SSA relative to its unfunctionalized equivalent (Sample 2), from 367 to 310 m^2g^{-1}, which may be due to tube rebundling, degradation, and/or functional groups blocking the pore openings.

Surface area as an exposure metric

Although there currently is no consensus regarding the most relevant exposure metric(s) for CNTs/CNFs, toxicological findings have prompted interest in workplace monitoring of nanoaerosol surface area. A BET analysis can be readily applied to bulk powders (e.g. to characterize CNTs for toxicological studies), but not to workplace monitoring at low concentrations. Various portable instruments, typically 'diffusion-charger'-(DC) based instruments reported to measure 'active surface area,' have been employed (Brouwer *et al.*, 2009; Elihn and Berg, 2009; Park *et al.*, 2009; Evans *et al.*, 2010; Bau *et al.*, 2011; LeBouf *et al.*, 2011), but it is unclear what these instruments actually measure in the field.

Correlation between BET- and DC-based results is not straightforward, especially for polydisperse aerosols containing larger particles (Ku and Kulkarni, 2012). Aerosols of CNT and CNF, and other nanomaterial powders, contain micrometer-sized agglomerates, which differ significantly from the 'ideal' aerosols used for instrument calibration (Ku and Kulkarni, 2012). Nevertheless, DC-based instruments have been applied to field studies on nanomaterials (Ntziachristos *et al.*, 2007; Brouwer *et al.*, 2009; Elihn and Berg, 2009; Buonanno *et al.*, 2010; Evans *et al.*, 2010). Most studies neglect to mention that a DC-based (active) surface area is not the same as BET (specific) surface area, and the instrument often is applied beyond the applicable particle size range (Ku and Kulkarni, 2012). A DC instrument gave results comparable to the geometric surface area for silver agglomerates <100 nm, but for agglomerates in the 100–200 nm size range, it underestimated the geometric surface area (Ku and Maynard, 2005). In another study, the DC-based surface area for spherical particles deviated significantly from the geometric surface area as the particle size increased to 900 nm (Ku, 2009, 2010). In a related study, the response of three DC instruments substantially underestimated the geometric surface area of submicrometer particles, by a factor of 3–10, with disagreement being greatest for larger particle agglomerates (Ku and Kulkarni, 2012). Even larger differences could be expected for complex aerosols such as CNTs and CNFs. These studies emphasize the problems in interpreting results of DC-based instruments, even when interferences are absent.

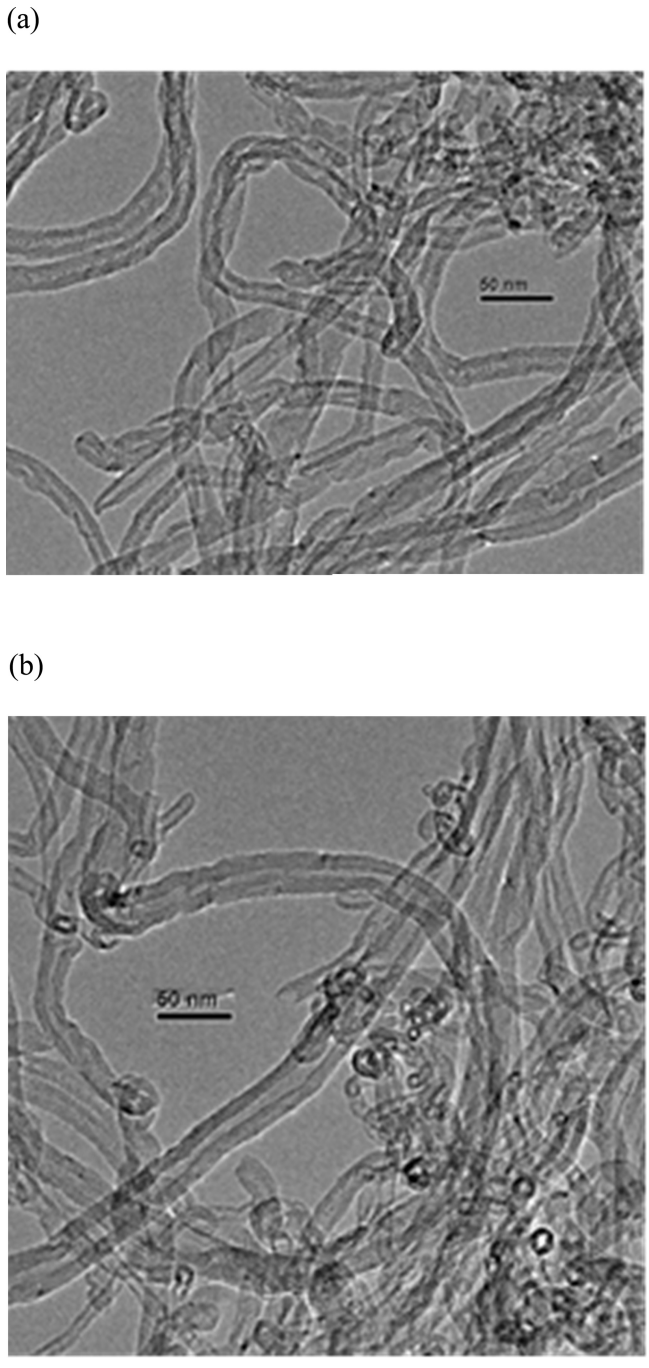

Fig. 5. TEM images of MWCNTs Sample 6 (a) and Sample 18 (b). Sample 18 shows more open-ended MWCNTs than Sample 6, which may explain its larger surface area.

The utility of direct-reading instruments for workplace monitoring of nanomaterials has been reported (e.g. Old and Methner, 2008; Methner *et al*., 2010); however, in our work (Evans *et al*., 2010; Birch *et al*., 2011; Dahm *et al*., 2012), direct-reading instruments have not been useful for monitoring CNTs and CNFs (or nanomaterial powders generally) because they lack adequate

sensitivity and selectivity. In our field studies, direct-reading instruments mainly have been used as indicators of background ultrafine aerosols, which are often present. Thus, even if reliable, sensitive, direct-reading instruments for monitoring aerosol surface area concentration were available, interference of other aerosols is a common problem that precludes accurate field measurement of nanomaterial surface area.

CONCLUSIONS

SSA can provide insight on the varied properties of CNTs and is a useful indicator of sample purity and homogeneity. The materials examined have a wide range of surface areas. Measured surface areas differed from product specifications, to varying degrees, and between similar products. For example, comparable SWCNT products with similar reported SSAs (near 400 m^2g^{-1}) had measured values of 662 m^2g^{-1} (Sample 1) and 367 m^2g^{-1} (Sample 2). Higher residual ash and metal content were found in the latter material, which lowers the SSA. Thus, the measured SSA was predictive of the different CNT purities of these materials. Electron microscopy and other analyses provided supporting data in identifying properties that influence SSA, including tube diameter, material defects, tube bundling, metals, and other carbonaceous matter.

Surface area is one of several metrics thought to be relevant to nanomaterial exposure, based on inhalation studies of some insoluble, fine/nanoscale particles. Though suppliers often provide SSAs and other data, thorough material characterization is needed. Results may differ from vendor specifications, sometimes substantially, and other key information (e.g. metals, amorphous carbon, and other CNT impurities; tube length and diameter) may be inaccurate or lacking. Comparisons between studies of materials that ostensibly have the same properties may be confounded if based on inaccurate/inadequate specifications. Thorough characterization is needed to account for differences that may affect toxicity and other research findings. This is especially important for *in vitro* studies, where very specific particle properties are examined with respect to specific toxicity endpoints.

Currently, there is no standardized method to measure the SSA concentration of workplace nanomaterial aerosols. Even if such methods existed, interference of other aerosols is a common problem. However, a sample of the bulk material(s) often can be obtained at the worksite. Multiple analyses can then be performed to more fully characterize the materials to which workers are exposed. A better understanding of the range of properties and toxicities of commercial CNTs and CNFs is needed to ensure health protective standards.

Although SSA provides useful information, the potential toxicity of CNTs and CNFs more likely relates to their fibrous structure and degree of agglomeration/bundling, perhaps in combination with residual metal and organic contents. Research on dose–response relationships is needed to determine what metrics are most appropriate for different types of nanomaterials. Ultimately, any metrics applied to occupational monitoring must be adequately sensitive and selective so that health risks based on exposure data can be accurately assessed.

SUPPLEMENTARY DATA

Supplementary data can be found at http://annhyg.oxfordjournals.org/.

Acknowledgements—The authors would like to thank Drs Bon Ki Ku, Pramod S. Kulkarni, and Leonid A. Turkevich for their helpful discussions.

Disclaimer—The findings and conclusions in this paper are those of the authors and do not necessarily represent the views of the National Institute for Occupational Safety and Health. Mention of company name or product does not constitute endorsement by the Centers for Disease Control and Prevention.

REFERENCES

Agnihotri S, Mota JP, Rostam-Abadi M *et al.* (2005) Structural characterization of single-walled carbon nanotube bundles by experiment and molecular simulation. Langmuir; 21: 896–904.

Andrews R, Jacques D, Qian D *et al.* (2001) Purification and structural annealing of multiwalled carbon nanotubes at graphitization temperatures. Carbon; 39: 1681–7.

Bau S, Witschger O, Gensdarmes F *et al.* (2011) Response of three instruments devoted to surface-area for monodisperse and polydisperse aerosols in molecular and transition regimes. J Phys: Conf Ser; 304: 012015.

Birch ME. (2003) Monitoring of diesel particulate exhaust in the workplace. In Schlecht PC, O'Connor PF, editors. NIOSH manual of analytical methods (NMAM). Third supplement to NMAM. 4th edn. Cincinnati, OH: Department of Health and Human Services, Public Health Service, Center for Disease Control and Prevention, National Institute for Occupational Safety and Health. DHHS (NIOSH) Publication No. 2003-154. Chapter Q.

Birch ME, Ku BK, Evans DE *et al.* (2011) Exposure and emissions monitoring during carbon nanofiber production–Part I: elemental carbon and iron-soot aerosols. Ann Occup Hyg; 55: 1016–36.

Brouwer D, van Duuren-Stuurman B, Berges M *et al.* (2009) From workplace air measurement results toward estimates of exposure? Development of a strategy to assess exposure to manufactured nano-objects. J Nanopart Res; 11: 1867–81.

Brown DM, Wilson MR, MacNee W *et al.* (2001) Size-dependent proinflammatory effects of ultrafine polystyrene particles: a role for surface area and oxidative stress in the enhanced activity of ultrafines. Toxicol Appl Pharmacol; 175: 191–9.

Buonanno G, Morawska L, Stabile L *et al.* (2010) Exposure to particle number, surface area and PM concentrations in pizzerias. Atmos Environ; 44: 3963–9.

Byl O, Liu J, Yates JT Jr. (2005) Etching of carbon nanotubes by ozone–a surface area study. Langmuir; 21: 4200–4.

Chakraborty S, Chattopadhyay J, Peng H *et al.* (2006) Surface area measurement of functionalized single-walled carbon nanotubes. J Phys Chem B; 110: 24812–5.

Chen C, Wang X. (2006) Adsorption of Ni(II) from aqueous solution using oxidized multiwall carbon nanotubes. Ind Eng Chem Res; 45: 9144–9.

Chen M, Yu HW, Chen JH *et al.* (2007) Effect of purification treatment on adsorption characteristics of carbon nanotubes. Diam Relat Mater; 16: 1110–5.

Cinke M, Li J, Chen B *et al.* (2002) Pore structure of raw and purified HiPco single-walled carbon nanotubes. Chem Phys Lett; 365: 69–74.

Dahm MM, Evans DE, Schubauer-Berigan MK *et al.* (2012) Occupational exposure assessment in carbon nanotube and nanofiber primary and secondary manufacturers: mobile direct-reading sampling. Ann Occup Hyg; 57: 328–44.

Delpeux-Ouldriane S, Szostak K, Frackowiak E *et al.* (2006) Annealing of template nanotubes to well-graphitized multi-walled carbon nanotubes. Carbon; 44: 799–823.

Donaldson K, Aitken R, Tran L *et al.* (2006) Carbon nanotubes: a review of their properties in relation to pulmonary toxicology and workplace safety. Toxicol Sci; 101: 179–80.

Du W, Wilson L, Ripmeester J *et al.* (2002) Investigation of the pore structure of as-prepared and purified HiPco single-walled carbon nanotubes by N2/Ar adsorption – implication for H2 storage. Nano Lett; 2: 343–6.

Elihn K, Berg P. (2009) Ultrafine particle characteristics in seven industrial plants. Ann Occup Hyg; 53: 475–84.

Endo M, Hayashi T, Kim YA *et al.* (2004) Applications of carbon nanotubes in the twenty-first century. Philos Trans A Math Phys Eng Sci; 362: 2223–38.

Eswaramoorthy M, Sen R, Rao C. (1999) A study of micropores in single-walled carbon nanotubes by the adsorption of gases and vapors. Chem Phys Lett; 304: 207–10.

Evans DE, Ku BK, Birch ME *et al.* (2010) Aerosol monitoring during carbon nanofiber production: mobile direct-reading sampling. Ann Occup Hyg; 52: 9–21.

Fujiwara A, Ishii K, Suematsu H *et al.* (2001) Gas adsorption in the inside and outside of single-walled carbon nanotubes. Chem Phys Lett; 336: 205–11.

Hemraj-Benny T, Bandosz TJ, Wong SS. (2008) Effect of ozonolysis on the pore structure, surface chemistry, and bundling of single-walled carbon nanotubes. J Colloid Interface Sci; 317: 375–82.

Hsieh SF, Bello D, Schmidt DF *et al.* (2012) Biological oxidative damage by carbon nanotubes: fingerprint or footprint? Nanotoxicology; 6: 61–76.

Kayiran S, Lamari F, Levesque D. (2004) Adsorption properties and structural characterization of activated carbons and nanocarbons. J Phys Chem B; 108: 15211–5.

Kondratyuk P, Yates JT Jr. (2007) Molecular views of physical adsorption inside and outside of single-wall carbon nanotubes. Acc Chem Res; 40: 995–1004.

Ku BK. (2009). Diffusion charger-based aerosol surface-area monitor response to airborne spherical particles 100–800 nm in diameter. In Proceedings of the Abstracts of the 4th International Conference on Nanotechnology—Occupational and Environmental Health. August 25–29, Helsinki, Finland: Finnish Institute of Occupational Health, p. 46.

Ku BK. (2010). Determination of the ratio of diffusion charging-based surface area to geometric surface area for spherical particles in the size range of 100–900 nm. J Aerosol Sci; 41: 835–47.

Ku BK, Kulkarni P. (2012) Comparison of diffusion charging and mobility-based methods for measurement of aerosol agglomerate surface area. J Aerosol Sci; 47: 100–10.

Ku BK, Maynard AD. (2005). Comparing aerosol surface-area measurement of mono disperse ultrafine silver agglomerates using mobility analysis, transmission electron microscopy and diffusion charging. J Aerosol Sci; 36: 1108–24.

Lam CW, James JT, McCluskey R *et al.* (2004) Pulmonary toxicity of single-wall carbon nanotubes in mice 7 and 90 days after intratracheal instillation. Toxicol Sci; 77: 126–34.

LeBlanc AJ, Moseley AM, Chen BT *et al.* (2010) Nanoparticle inhalation impairs coronary microvascular reactivity via a local reactive oxygen species-dependent mechanism. Cardiovasc Toxicol; 10: 27–36.

LeBouf RF, Ku, BK, Chen BT *et al.* (2011) Measuring surface area of airborne titanium dioxide powder agglomerates: relationships between gas adsorption diffusion and mobility-based methods. J Nanopart Res; 13: 7029–39.

Li F, Wang Y, Wang D *et al.* (2004) Characterization of single-wall carbon nanotubes by N2 adsorption. Carbon; 42: 2375–83.

Li Y, Wang S, Luan Z *et al.* (2003) Adsorption of cadmium(II) from aqueous solution by surface oxidized carbon nanotubes. Carbon; 41: 1057–62.

Lison D, Lardot C, Huaux F *et al.* (1997) Influence of particle surface area on the toxicity of insoluble manganese dioxide dusts. Arch Toxicol; 71: 725–9.

Lison D, Muller J. (2008) Lung and systemic responses to carbon nanotubes (CNT) in mice. Toxicol Sci; 101: 179–80.

Lux Research. (2007) The nanotech report. 5th edn. New York, NY: Lux Research.

Mackie E, Wolfson R, Arnold L *et al.* (1997) Adsorption studies of methane films on catalytic carbon nanotubes and on carbon filaments. Langmuir; 13: 7197–201.

Martinez M, Callejas M, Benito A *et al.* (2003) Sensitivity of single wall carbon nanotubes to oxidative processing: structural modification, intercalation and functionalization. Carbon; 41: 2247–56.

Mercer RR, Hubbs AF, Scabilloni JF *et al.* (2011) Pulmonary fibrotic response to aspiration of multi-walled carbon nanotubes. Part Fibre Toxicol; 8: 21.

Mercer RR, Scabilloni JF, Wang L *et al.* (2009) Use of labeled single walled carbon nanotubes to study translocation from the lungs. The Toxicologist; 108: A2192.

Methner M, Hodson L, Geraci C. (2010) Nanoparticle emission assessment technique (NEAT) for the identification and measurement of potential inhalation exposure to engineered nanomaterials–part A. J Occup Environ Hyg; 7: 127–32.

Milne WI, Mann M, Dijon J *et al.* (2008) Carbon nanotubes. E-Nano Newsletter; 13: 5–32.

Monteiller C, Tran L, MacNee W *et al.* (2007) The pro-inflammatory effects of low-toxicity low-solubility particles, nanoparticles and fine particles, on epithelial cells in vitro: the role of surface area. Occup Environ Med; 64: 609–15.

Montoro L, Rosolen J. (2004) A multi-step treatment to effective purification of single-walled carbon nanotubes. Carbon; 44: 3293–301.

Muller J, Huaux F, Moreau N *et al.* (2005) Respiratory toxicity of multi-wall carbon nanotubes. Toxicol Appl Pharmacol; 207: 221–31.

Murray AR, Kisin ER, Tkach AV *et al.* (2012) Factoring-in agglomeration of carbon nanotubes and nanofibers for better prediction of their toxicity versus asbestos. Part Fibre Toxicol; 9: 10.

Naseh M, Khodadadi A, Mortazavi Y *et al.* (2009) Functionalization of carbon nanotubes using nitric acid oxidation and DBD plasma. Int J Chem Biol Eng; 37: 177–9.

Nel A, Xia T, Mädler L *et al.* (2006) Toxic potential of materials at the nanolevel. Science; 311: 622–7.

Ning G, Wei F, Luo G *et al.* (2005) Online BET analysis of single-wall carbon nanotube growth and its effect on catalyst reactivation. Carbon; 43: 1439–44.

Ntziachristos L, Polidori A, Phuleria H *et al.* (2007) Application of a diffusion charger for the measurement of particle surface concentration in different environments. Aerosol Sci Tech; 41: 571–80.

Nurkiewicz TR, Porter DW, Hubbs AF *et al.* (2009) Pulmonary nanoparticle exposure disrupts systemic microvascular nitric oxide signaling. Toxicol Sci; 110: 191–203.

Oberdörster G, Maynard A, Donaldson K *et al.* (2005) Principles for characterizing the potential human health effects from exposure to nanomaterials: elements of a screening strategy. Part Fibre Toxicol; 2: 8.

Old L, Methner MM. (2008) Engineering case report: effectiveness of local exhaust ventilation (LEV) in controlling engineered nanomaterial emissions during reactor cleanout operations. J Occup Environ Hyg; 5: D63–9.

Park JY, Raynor PC, Maynard AD *et al.* (2009) Comparison of two estimation methods for surface area concentration using number concentration and mass concentration of combustion-related ultrafine particles. Atmos Environ; 43: 502–9.

Park T, Banerjee S, Hemraj-Benny T *et al.* (2006) Purification strategies and purity visualization techniques for single-walled carbon nanotubes. J Mater Chem; 16: 141–54.

Pauluhn J. (2010) Subchronic 13-week inhalation exposure of rats to multiwalled carbon nanotubes: toxic effects are determined by density of agglomerate structures, not fibrillar structures. Toxicol Sci; 113: 226–42.

Peigney A, Laurent C, Flahaut E *et al.* (2001) Specific surface area of carbon nanotubes and bundles of carbon nanotubes. Carbon; 39: 507–14.

Plata DL, Gschwend PM, Reddy CM. (2008) Industrially synthesized single-walled carbon nanotubes: compositional data for users, environmental risk assessments, and source apportionment. Nanotechnology; 19: 185706.

Poland CA, Duffin R, Kinloch I *et al.* (2008) Carbon nanotubes introduced into the abdominal cavity of mice show asbestos-like pathogenicity in a pilot study. Nat Nanotechnol; 3: 423–8.

Porter DW, Hubbs AF, Mercer RR *et al.* (2010) Mouse pulmonary dose- and time course-responses induced by exposure to multi-walled carbon nanotubes. Toxicology; 269: 136–47.

Raymundo-Pinero E, Azais P, Cacciaguerra T *et al.* (2005) KOH and NaOH activation mechanisms of multiwalled carbon nanotubes with different structural organization. Carbon; 43: 786–95.

Raymundo-Pinero E, Cazorla-Amoros D, Linares-Solano A *et al.* (2002) High surface area carbon nanotubes prepared by chemical activation. Carbon; 40: 1614–7.

Reid CR, Thomas KM. (1999) Adsorption of gases on a carbon molecular sieve used for air separation: linear adsorptives as probes for kinetic selectivity. Langmuir; 15: 3206–18.

Sager TM, Castranova V. (2009) Surface area of particle administered versus mass in determining the pulmonary toxicity of ultrafine and fine carbon black: comparison to ultrafine titanium dioxide. Part Fibre Toxicol; 6: 15.

Shvedova AA, Castranova V, Kisin ER *et al.* (2003) Exposure to carbon nanotube material: assessment of nanotube cytotoxicity using human keratinocyte cells. J Toxicol Environ Health A; 66: 1909–26.

Shvedova AA, Kisin E, Murray AR *et al.* (2008) Inhalation vs. aspiration of single-walled carbon nanotubes in C57BL/6 mice: inflammation, fibrosis, oxidative stress, and mutagenesis. Am J Physiol Lung Cell Mol Physiol; 295: L552–65.

Shvedova AA, Kisin ER, Mercer R *et al.* (2005) Unusual inflammatory and fibrogenic pulmonary responses to single-walled carbon nanotubes in mice. Am J Physiol Lung Cell Mol Physiol; 289: L698–708.

Singh S, Shi T, Duffin R *et al.* (2007) Endocytosis, oxidative stress and IL-8 expression in human lung epithelial cells upon treatment with fine and ultrafine TiO2: role of the specific surface area and of surface methylation of the particles. Toxicol Appl Pharmacol; 222: 141–51.

Stoeger T, Reinhard C, Takenaka S *et al.* (2006) Instillation of six different ultrafine carbon particles indicates a surface area threshold dose for acute lung inflammation in mice. Environ Health Perspect; 114: 328–33.

Tran CL, Buchanan D, Cullen RT *et al.* (2000) Inhalation of poorly soluble particles. II. Influence Of particle surface area on inflammation and clearance. Inhal Toxicol; 12: 1113–26.

Tsang S, Harris P, Green M. (1993) Thinning and opening of carbon nanotubes by oxidation using carbon dioxide. Nature; 362: 520–3.

WTEC. (2007) WTEC panel report on international assessment of research and development of carbon nanotubes manufacturing and applications. Final Report. Baltimore, MD: World Technology Evaluation Center (WTEC). Available at http://www.wtec.org/cnm/CNM_final_report.pdf. Accessed 7 August 2013.

Ye J, Liu X, Cui H *et al.* (2005) Electrochemical oxidation of multi-walled carbon nanotubes and its application to electrochemical double layer capacitors. Electrochem Commun; 7: 249–55.

Yin Y, Mays T, McEnaney B. (1999) Adsorption of nitrogen in carbon nanotube arrays. Langmuir; 15: 8714–8.

Zacharia R, Kim K, Hwang S *et al.* (2007) Intrinsic linear scaling of hydrogen storage capacity of carbon nanotubes with the specific surface area. Catal Today; 120: 426–31.

Zhu W, Miser D, Chan W *et al.* (2003) Characterization of multiwalled carbon nanotubes prepared by carbon arc cathode deposit. Mat Chem Phys; 82: 638–47.